Effects of Substrate Analogues and pH on Manganese Superoxide Dismutases[†]

Leandro C. Tabares,[‡,§] Néstor Cortez,[§] B. Yukihiro Hiraoka,[||] Fumiyuki Yamakura,[#] and Sun Un*[,‡]

Service de Bioénergétique, DBJC, CNRS URA 2096, CEA Saclay, 91191 Gif-sur-Yvette, France, Instituto de Biologia Molecular y Celular de Rosario (IBR), Universidad Nacional de Rosario and CONICET, Suipacha 531, S2002LRK Rosario, Argentina, Institute for Oral Science, Matsumoto Dental University, Shiojiri 399-0781, Japan, and Departament of Chemistry, School of Medicine, Juntendo University, 1-1 Hiragagakuendai, Chiba 2701695, Japan

Received September 27, 2005; Revised Manuscript Received December 12, 2005

ABSTRACT: The effect of the substrate analogues azide and fluoride on the manganese(II) zero-field interactions of different manganese-containing superoxide dismutases (SOD) was measured using high-field electron paramagnetic resonance spectroscopy. Two cambialistic types, proteins that are active with manganese or iron, were studied along with two that were only active with iron and another that was only active with manganese. It was found that azide was able to coordinate directly to the pentacoordinated Mn(II) site of only the MnSOD from *Escherichia coli* and the cambialistic SOD from *Rhodobacter capsulatus*. The formation of a hexacoordinate azide-bound center was characterized by a large reduction in the Mn(II) zero-field interaction. In contrast, all five SODs were affected by fluoride, but no evidence for hexacoordinate Mn(II) formation was detected. For both azide and fluoride, the extent of binding was no more than 50%, implying either that a second binding site was present or that binding was self-limiting. Only the Mn(II) zero-field interactions of the two SODs that had little or no activity with manganese were found to be significantly affected by pH, the manganese-substituted iron superoxide dismutase from *E. coli* and the Gly155Thr mutant of the cambialistic SOD from *Porphyromonas gingivalis*. A model for anion binding and the observed p*K* involving tyrosine-34 is presented.

Superoxide dismutases (SOD[1]) are enzymes that play a key role in cellular protection against oxidative stress conditions. They catalyze the disproportionation of superoxide to form molecular oxygen and hydrogen peroxide (*1*, *2*) through a cyclic oxidation−reduction mechanism involving a metal cofactor (*3*−*5*). Four families of SODs are distinguished by their native metal ion: manganese, iron, copper−zinc (*1*), and nickel (*6*, *7*).

Although iron and manganese SODs exhibit high structural homology (*8*−*11*), their activities are highly metal-specific (*12*, *13*), and only a small subgroup of so-called "cambialistic" SODs are active with either metal ion (*14*−*18*). Among the Fe- and MnSODs, the metal is coordinated in the equatorial plane by two histidines and an aspartic acid and in the axial positions by a histidine and a solvent molecule forming an unusual trigonal bipyramidal geometry (Figure 1). The axial solvent molecule is thought to be an hydroxide anion in the oxidized form of the enzyme and a water in the reduced form (*8*, *9*). This solvent molecule hydrogen-bonds both the aspartate ligand and the amide side chain of a nearby glutamine-146 (*Escherichia coli* MnSOD amino acid numbering is used throughout this work) that in turn donates a hydrogen bond to the highly conserved tyrosine-34 residue (Tyr34). These amino acids are part of an extended hydrogen-bonding network that is thought to be important for the activity, by controlling proton motion and determining the p*K* of the active site.

Fe- and MnSODs have characteristic pH dependences. FeSODs have a p*K* of approximately 8.5 that is associated with a decrease in activity at high pH (*3*). In the case of the oxidized enzyme, this p*K* has been attributed to hydroxide binding to the Fe(III) center (*19*, *20*), while in the reduced state (Fe(II)SODs), a similar p*K* has been assigned to the deprotonation of Tyr34 (*21*−*23*). Kinetic measurements on MnSODs indicate a p*K* of 9.4−9.8 (*24*, *25*). For the oxidized state (Mn(III)SODs), Borgstahl (*26*) and Whittaker (*27*) have proposed that the observed p*K* between 9.4 and 10.1 corresponds to hydroxide binding to the metal, while others have argued that it is due to Tyr34 deprotonation (*23*, *25*, *28*, *29*). By contrast, the pH dependence of the Mn(II) oxidation state has not been extensively studied. A p*K* of 10.7 for EcMn(II)SOD has been assigned to the deprotonation of Tyr34 using Resonance Raman spectroscopy (*29*). However, the 9 GHz EPR spectra also suggested that there

[†] This project was supported in part by CONICET, SeTCIP, and ANPCyT of Argentina and the ECOS Sud/SeCyT collaboration program (Project A02B01).

* Corresponding author. Phone, 33 1 69082842; fax, 33 1 69088717; e-mail, sun@ozias.saclay.cea.fr.

[‡] Service de Bioénergétique, DBJC, CNRS.

[§] Universidad Nacional de Rosario and CONICET.

[||] Matsumoto Dental University.

[#] Juntendo University.

[1] Abbreviations: SOD, superoxide dismutase; MnSOD, manganese superoxide dismutase; FeSOD, iron superoxide dismutase; EcMnSOD, *Escherichia coli* manganese superoxide dismutase; EcFeSOD, *E. coli* iron superoxide dismutase; EcMn(Fe)SOD, *E. coli* manganese-substituted iron superoxide dismutase; RcMnSOD, *Rhodobacter capsulatus* manganese superoxide dismutase; PgMnSOD-WT, *Porphyromonas gingivalis* manganese superoxide dismutase; PgMnSOD-G155T, mutant of *Porphyromonas gingivalis* manganese superoxide dismutase in which Gly155 has been replaced by a threonine; EPR, electron paramagnetic resonance; HFEPR, high-field EPR; NPB, nonprotein bound; PCM, point-charge model; Tris, Tris(hydroxymethyl)aminomethane; Caps, *N*-cyclohexyl-3-aminopropanesulfonic acid; EDTA, ethylenediaminetetraacetic acid.

10.1021/bi051947m CCC: $33.50
Published on Web 01/24/2006

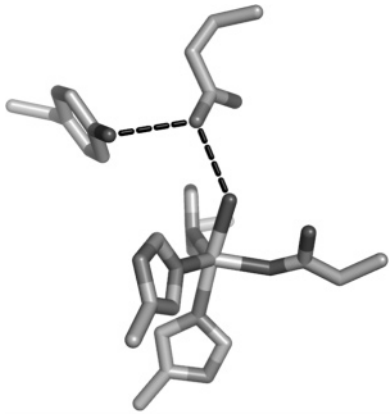

FIGURE 1: Structure of the MnSOD metal site. The Mn ion is coordinated by an Asp and two His in the equatorial plane and another His and a solvent molecule in the axial positions. Glutamine-146 and tyrosine-34, which are part of the hydrogen-bound network, are also shown.

were changes in the electronic structure of the Mn(II) center at about the same pH (*29*).

In addition to pH, Fe- and MnSODs are also affected by small anionic substrate analogues, such as azide and fluoride. These two analogues also act as competitive inhibitors of the activity (*3*, *20*, *30*−*34*). It has been shown that they are able to directly coordinate to the Fe(III)SOD centers (*30*, *35*). In contrast, there is no evidence for direct coordination of these analogues to the reduced Fe(II)SOD metal center, even at very high concentrations (*36*, *37*). However, Fe(II)-SOD has been shown to bind fluoride probably near Tyr34, implying that the reductive half-reaction might proceed through an outer-sphere mechanism (*9*, *37*). A hexacoordinate azide−MnSOD complex has been observed in the crystal structure of the *Thermus thermophilus* protein (*30*). However, spectroscopic studies have shown that azide binding is temperature-dependent. Although earlier studies have suggested that azide binds at room temperature with conservation of coordination number, with the metal remaining pentacoordinate (*38*), Jackson and co-workers have recently shown that the room-temperature spectrum can be assigned to an outer-sphere azide−SOD complex which is transformed into an inner-sphere hexacoordinated azide−SOD complex at low temperatures (*39*). These measurements in conjunction with others suggest a prebinding site for the superoxide that is likely to be near Tyr34 (*9*, *19*). In our preliminary work, we exploited high-magnetic field EPR (HFEPR) to confirm unambiguously that at cryogenic temperatures azide does bind directly to the Mn(II) centers in *E. coli* and *Rhodobacter capsulatus* SODs forming hexacoordinate metal centers (*40*).

The magnetic zero-field interaction of Mn(II) ions in manganese-reconstituted Fe- and MnSODs can be used to monitor changes in the coordination number of metal ion, as well as to detect more subtle changes in the protein environment (*41*, *42*). Accurate measurements of the Mn(II) zero-field interaction can be readily made using HFEPR. The Mn(II) EPR spectra are determined by the spin Hamiltonian:

$$H = \beta\vec{B}\cdot\boldsymbol{g}\cdot\vec{S} + \vec{I}\cdot\mathbf{A}\cdot\vec{S} + \frac{D}{3}(3S_z^2 - S(S+1)) + \frac{E}{2}(S_+^2 + S_-^2) \quad (1)$$

Equation 1 describes the energies and wave functions of the six electronic spin states where the first term describes the electronic Zeeman interaction and the second the hyperfine interaction (A) between the unpaired electrons ($S = 5/2$) and the manganese nucleus ($I = 5/2$). Within the experimental accuracy of the high-field measurements, the Mn(II) centers in SODs have g and A values that are isotropic with values of 2.0009 and 0.240 GHz, respectively (*41*). The last two terms of eq 1 represent the zero-field interaction, described by the axial, D, and rhombic, E, parameters. The zero-field D and E parameters vary significantly among the different Mn(II)SODs ranging from 10.1 to 10.8 GHz for the former and 0.2 to 0.9 GHz for the latter (*41*).

Azide addition to the *R. capsulatus* and *E. coli* Mn(II)-SOD samples has been shown to lead to a large reduction in the Mn(II) zero-field interaction to 1.4 GHz due to the formation of a hexacoordinate Mn(II) center (*40*). At high magnetic fields, the second-order zero-field contributions became smaller than the hyperfine coupling leading to the appearance of six evenly spaced sharp resonances separated by the hyperfine coupling, A, and centered near the magnetic field corresponding to the free electron g-value (2.00232 or 10.16 T at an observation frequency of 285 GHz).

We have expanded upon our preliminary HFEPR work on azide binding to SODs, by including the manganese and the manganese-substituted iron SODs from *E. coli* (EcMn-SOD and EcMn(Fe)SOD, respectively), as well as the cambialistic SOD from *R. capsulatus* (RcMnSOD) which exhibits higher activity with manganese than with iron (*18*), the fully cambialistic SOD from *Porphyromonas gingivalis* that is equally active with iron and manganese (PgMnSOD-WT), and a mutant of this latter protein in which the glycine-155 has been substituted with a threonine (PgMnSOD-G155T) (*43*). This latter mutation converted the cambialistic protein to an iron-dependent one. To establish a more complete picture of analogue binding and inhibition, we also examined the effects of the fluoride binding. These studies were complemented with a complete pH study of the five SODs.

EXPERIMENTAL PROCEDURES

Samples. *E. coli* Mn- and FeSODs were purchased from Sigma-Aldrich. The SODs were washed several times with 1 mM EDTA in 10 mM Tris-HCl buffer, pH 7.8, to remove any adventitious manganese ions. Manganese(II) substitution into EcFeSOD is described in ref *41*. Preparations of RcMnSOD, PgMnSOD, and PgMnSOD-Gly155Thr are described separately in other communications (*18*, *43*, *44*). Spectra were obtained from protein samples containing 10 mM Tris-HCl, pH 7.8, and 0.1 mM EDTA. For analogue binding studies, the buffer contained 10 mM Tris, pH 7.8, and fluoride or azide added from a 500 mM stock solution, but no EDTA was added. For pH studies, 10 mM Tris-HCl containing 0.1 mM EDTA was used between pH 7.5 and 9, and 100 mM CAPS without EDTA between pH 9.5 and 11. The samples were flash-frozen in liquid nitrogen before spectra were taken. Adventitious Mn(II) ions and exogenous ligands were removed from the samples using a 5 mL desalting column (Hi-Trap, Amersham Biosciences). Ultrafiltrations were carried out using 30 kDa cutoff membrane filters (Centricon YM-30, Millipore Corporation).

Table 1: Percent of Inhibition of SOD Activity by Azide and Fluoride

enzyme	10 mM azide	10 mM fluoride
EcMnSOD	41 ± 5	31 ± 3
RcMnSOD	37 ± 3	30 ± 2
PgMnSOD-WT	31 ± 2	27 ± 3
PgMnSOD-G155T	29 ± 2	16 ± 3

Activity Measurements. Activity measurements were carried out using the standard assay of McCord and Fridovich (*45*) in 50 mM phosphate buffer, pH 7.8, at 25 °C. The inhibition of the activity by the substrate analogues was measured by addition of 10 mM azide or fluoride to a protein sample containing all of the required components except the xanthine oxidase, which was added to start the reaction after 10 min of sample incubation.

High-Field EPR Spectra. The spectrometer has been described in detail elsewhere (*46*). Field calibration was based on a Mn(II)-doped MgO standard ($g = 2.000101$) (*47*) sample, and the absolute error in field measurements was 1 G (0.1 mT) or 0.0001 in g. All spectra were obtained with 10 G modulation under nonsaturating conditions at 285 GHz with 5 G resolution at 25 K. The quality of spectra was such that they could be reliably reproduced and singly and doubly integrated.

Conventional 9 GHz spectra were obtained on a Bruker ESP300 EPR spectrometer equipped with an Oxford Instrument cryostat for sample temperature regulation and a Hewlett-Packard frequency counter for microwave frequency measurements.

Estimation of Zero-Field Parameters. We have shown that it is possible to obtain simulations that accurately reproduce the HFEPR spectra of SOD proteins (*41*, *42*). Error limits of the fitting procedure were ±0.06 GHz for the two zero-field parameters. However, some of the spectra encountered in this study arose from multiple centers that had distinct zero-field parameters that made these spectra difficult to simulate. In these cases, we used the edges of the spectra to estimate the zero-field parameter. The edges of the spectra are given to second-order (*48*) by $2(D + E)^2/(g\beta f_{mw})$ and $(7/2)D^2/(g\beta f_{mw}) + 11DE/(g\beta f_{mw})$ for low and high-field edges, respectively, and where f_{mw} is the microwave frequency, and other symbols have their normal meaning. By using these two equations and manually measuring the magnetic field positions of the edges, we were able to estimate the zero-field parameters. In test cases, this method yielded zero-field values that were within 0.20 GHz of those obtained by simulations.

Molecular structures were generated using the program PyMOL (Delano Scientific LLC, www.pymol.org).

RESULTS

Activity Measurements. The relative inhibitory effects of azide and fluoride on the activity of the four active proteins were assayed and are reported in Table 1. No measurement were made on EcMn(Fe)SOD, since it was known to be inactive (*49*). The enzymatic activities were inhibited by 29−41% with 10 mM azide (Table 1). The PgMnSOD-G155T, which had low but finite activity with manganese, was the least affected, while the two proteins, EcMnSOD and RcMnSOD, that directly bind azide (see below and ref *40*) to the metal centers, were the most affected. Fluoride inhibited the enzyme activities to a slightly lesser degree than azide, ranging from 16 to 31% (Table 1). The inhibition by fluoride followed the same trend as azide.

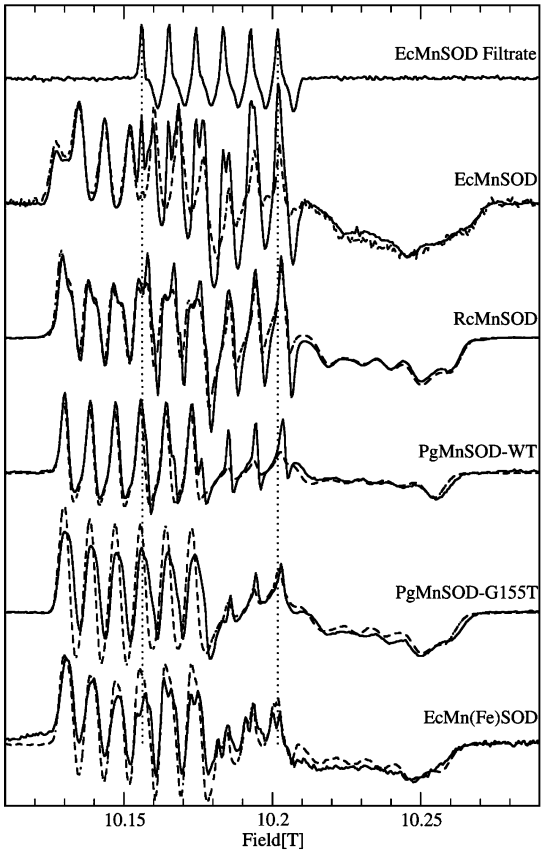

FIGURE 2: MnSOD HFEPR spectra at pH 7.8 (dash lines) and at high pH (solid lines, EcMnSOD, pH 10.8; RcMnSOD, pH 10.8; PgMnSOD-WT, pH 11.1; PgMnSODG155T, pH 10.8; EcMn(Fe)-SOD, pH 10.3). The spectrum of the filtrate of the pH 10.8 EcMnSOD sample containing nonprotein bound (NPB) Mn(II) is also shown (top).

Effect of pH. Of the five proteins studied, only EcMn(II)(Fe)SOD exhibited a strong pH dependence (Figure 2). The pH dependence of the four lowest-field EcMn(II)(Fe)SOD hyperfine resonances is shown in Figure 3. The spectra of this protein were pH-independent until pH 9, after which the hyperfine features became noticeably broadened. This broadening reached a maximum at about pH 10.3. The easiest quantifiable spectral features were the peak-to-trough amplitudes of the four resonances. A pH profile of the peak-to-trough amplitude of the first hyperfine line is shown in the inset of Figure 3. All four hyperfine features shown in the figure exhibited the same pH profile with a midpoint of approximately 9.8.

At the highest pH, a very broad low-field edge feature became evident (Figure 3). Unlike the resolved hyperfine features, this broad resonance was not titratable and not reproducible. Simultaneous simulations of the 285 and 190 GHz spectra at pH 10.8 were carried out (Figure 4). Although the quality of the fit was not as good as those we have previously reported, simultaneous fitting was sufficient to establish that $|D|$ decreased by about 0.30 GHz, while E increased by at least 0.10 GHz, leading to values of 10.209 and 0.485 (Table 2).

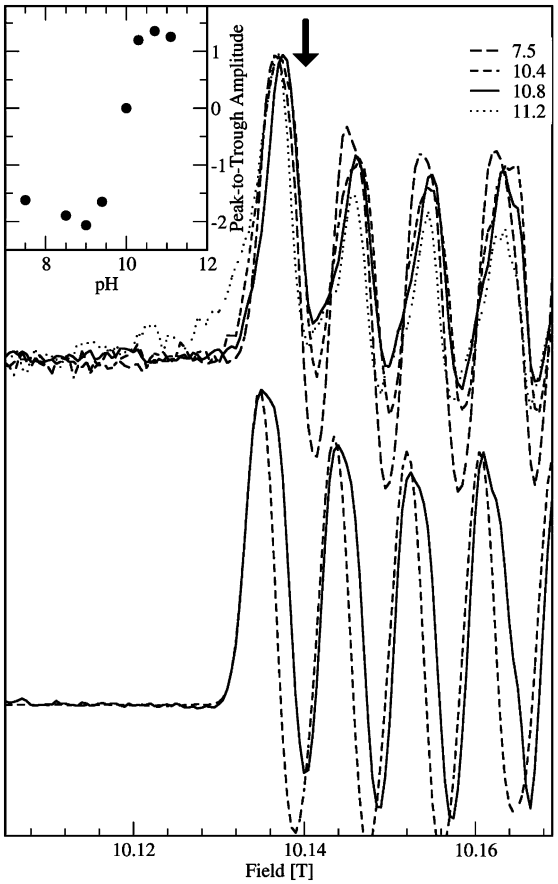

FIGURE 3: The pH dependence of the low-field hyperfine resonances of the EcMn(Fe)SOD (top) and PgMnSOD-G155T spectra (bottom, pH 7.8, in dash line, and pH 10.8, in solid line). The inset shows pH profile of the peak-to-trough amplitude of the lowest-field hyperfine resonance of the EcMn(II)(Fe)SOD spectra (indicated by the arrow).

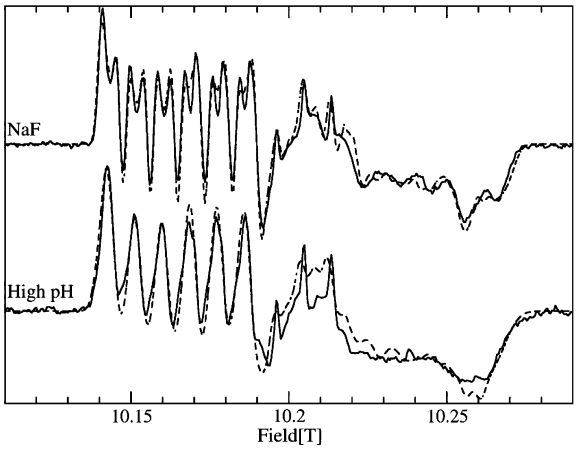

FIGURE 4: The HFEPR spectra (solid lines) of EcMn(II)(Fe)SOD in 10 mM Tris, pH 7.8, and 20 mM sodium fluoride (top) and 10 mM CAPS, pH 10.8 (bottom). Simulations are shown in dash lines.

The only other protein that exhibited any significant pH dependence was PgMnSOD-G155T. Similar to EcMn(Fe)-SOD, the low-field hyperfine lines of the mutant broadened with increasing pH. However, this effect was only evident above pH 10.8.

For the other three proteins, the only effect of increasing the pH was the concomitant increase in a narrow six-line signal in the center of the spectrum. This signal was found to correspond to nonprotein bound (NPB) Mn(II) ions released from the protein at high pH (Figure 2). NBP Mn(II) was a normal contamination in our samples; however, its fingerprint signal could be easily discriminated from the active site Mn(II) even in the cases where another six-line component arising from a Mn(II) protein center was present as was the case with some azide−Mn(II)SOD complex samples (see Supporting Information for an example). The presence of NPB Mn(II) could be easily tested by ultrafiltration of the sample using a 30 kDa cutoff membrane and recording the HFEPR spectra of the filtrate.

Table 2: The Mn(II) $|D|$ and E Parameters of the Five SODs in the Presence of Anions and at High pH[a]

	$\lvert D\rvert$	distribution in D	E	distribution in E
		EcMn(II)SOD		
native[b]	10.640	0.215	0.853	0.245
fluoride[c,d]	10.982	0.293	0.457	0.164
chloride/azide[e]	10.687	0.199	0.970	0.204
		RcMn(II)SOD		
native	10.775	0.103	0.508	0.146
fluoride[c,d]	10.785	0.216	0.626	0.124
		EcMn(II)(Fe)SOD		
native[b]	10.521	0.141	0.381	0.130
fluoride	10.287	0.133	0.578	0.132
high pH[c,f]	10.209	0.186	0.485	0.216
		PgMn(II)SOD-WT		
native[b]	10.699	0.110	0.240	0.113
		PgMn(II)SOD-G155T		
native[b]	10.754	0.137	0.368	0.165
high pH[f]	10.757	0.115	0.458	0.193

[a] The values were obtained by simulation of 285 GHz HFEPR spectra shown in Figures 2−7. Values are given in gigahertz. The estimate errors in $|D|$ and E were 0.06 GHz. Distributions were assumed to be Gaussian. [b] pH 8, 10 mM Tris. [c] From the simultaneous fit of the 190 and 285 GHz EPR spectra. [d] The putative fluoride spectra obtained by numerical decomposition of spectra obtained under partial binding conditions were simulated (see text for details). [e] The values were from the fitting of the of chloride data. The spectra of chloride and azide pentacoordinated Mn(II) adducts were essentially identical. For the zero-field parameters of the hexacoordinate azide complex, see ref *40*. [f] In each case, the pH is same as indicated in Figure 2.

In the case of EcMn(II)SOD, the conventional 9 GHz spectrum was also recorded at pH 8.2 in Tris buffer and pH 10.4 in CAPS buffer. The samples were freshly filtered and maintained at 4 °C so as to diminish the likelihood of metal release and to reduce the uncertainty in pH associated with sample freezing. Consistent with the HFEPR measurements and contrary to a previous study (*29*), the 9 GHz spectra showed no pH dependence (see Supporting Information for 9 GHz spectra). The 9 GHz high-pH spectrum of EcMnSOD in the presence of 0.5 mM Mn(II) and 1 mM EDTA exhibited a relatively sharp six-line component at a g-value of approximately 4, as well as a strong resonance at a g-value of 2 (see Supporting Information). The spectrum under these conditions was similar to the previously published high-pH spectrum (*29*).

Azide Addition. Figures 5 (left panel) and 6 (top) show the effect of the addition of 100 mM azide. As previously reported, azide addition to the EcMnSOD and RcMnSOD samples led to the appearance of a six-line fingerprint component associated with azide binding to the Mn(II) center (*40*). In addition to this substantial change, a subtle modification in the broad component corresponding to the native pentacoordinated centers was observed. This azide-dependent

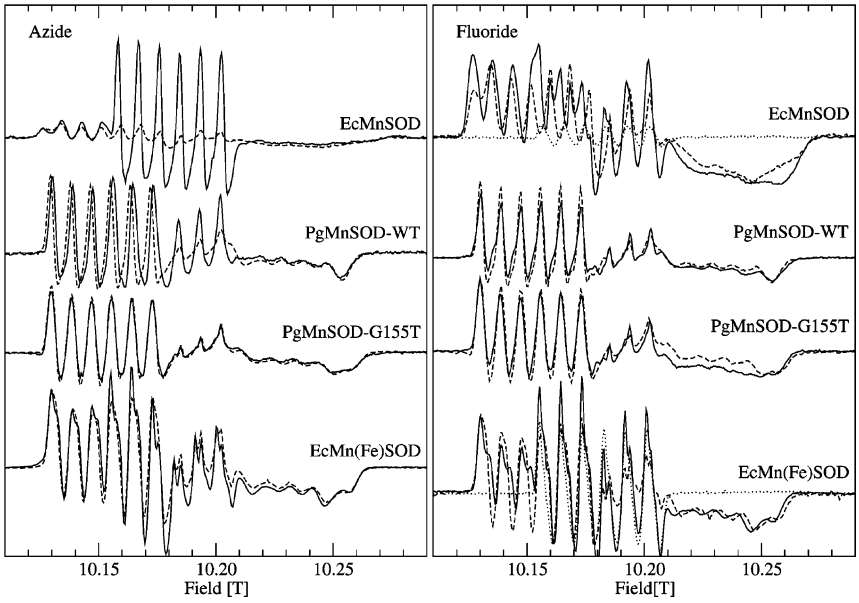

FIGURE 5: The HFEPR spectra of the different SODs in the presence of 100 mM sodium azide (left panel, solid lines) and 100 mM sodium fluoride, except for EcMn(Fe)SOD for which 20 mM fluoride was used (right panel, solid lines). The spectra in the absences of exogenous ligand are also shown (dash lines).

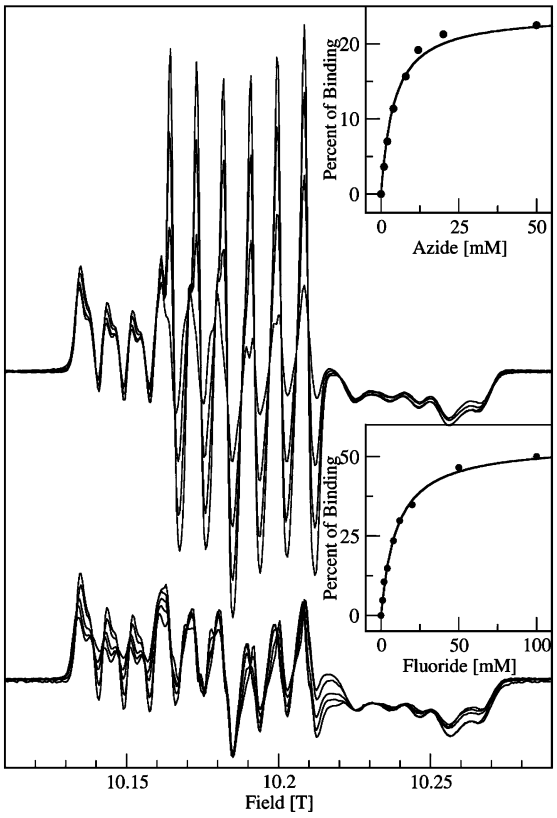

FIGURE 6: The dependence of the HFEPR RcMn(II)SOD spectra on azide (top) and fluoride (bottom) concentration. The insets show the percentage of analogue binding as a function of concentration (see text for details). The fits (solid lines) were obtained assuming a single binding-site model. The K_d was approximately 4 mM for azide and 9 mM for fluoride.

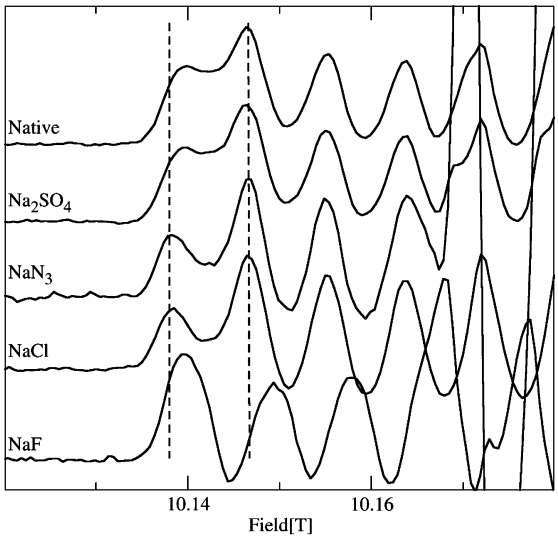

FIGURE 7: The effect of various sodium salts on the HFEPR spectra of EcMn(II)SOD. The sodium fluoride spectrum was obtained by decomposition analysis (see text for details). In each case, only the low-field portion is shown and the salt concentration was 100 mM.

modification was much more evident in the case of EcMn-(II)SOD (Figure 7). Because of the highly resolved nature of the HFEPR spectra, the azide binding curves could be easily generated from the normalized peak intensities of the six-line component. The much more laborious two-component spectral decomposition analysis using the spectrum of the free enzyme (broad component) and the azide complex (middle six-line component) yielded essentially the same result. At saturating azide concentrations, only 25% of the RcMn(II)SOD centers were bound with the analogue, while in case of EcMn(II)SOD (data not shown), the maximum binding was 20%. The apparent K_d based on a single-binding model was 4 mM for RcMn(II)SOD and 3 mM for EcMn-(II)SOD.

Unexpectedly, azide had only a minimal effect on the HFEPR spectra of PgMnSOD-WT, PgMnSOD-G155T, and EcMn(Fe)SOD, and none of these proteins exhibited the fingerprint six-line spectral component attributable to the hexacoordinate azide-Mn(II)SOD complex (Figure 5, left panel). The PgMn(II)SOD-G155T spectrum remained unchanged, while the PgMn(II)SOD-WT and EcMn(II)(Fe)-SOD spectra were only slightly modified. In the case of

PgMn(II)SOD-WT, the low-field hyperfine resonances were shifted to higher fields, while the high-field edge of the spectrum remained unchanged. These changes corresponded to a decrease in $|D|$ of about 0.30 GHz and an increase in E of about 0.10 GHz. For the EcMn(II)(Fe)SOD, a small high-field shoulder appeared on each of the low-field hyperfine resonances with slight changes in field positions.

Fluoride Addition. Fluoride affected the spectra of all five proteins (Figures 5, right panel and Figure 6, bottom) to varying degrees. Both PgMn(II)SOD proteins exhibited broadening of the high-field portions of the spectra. For RcMn(II)SOD and EcMn(II)(Fe)SOD, a new set of resonances was observed. The EcMn(II)SOD spectrum appeared to be completely changed by fluoride addition. The amplitudes and positions of the resolved low-field hyperfine features were modified, as well as the shape at the high-field edge. As with the azide addition, changes to the spectra of all five proteins were reversible, disappearing after removal of fluoride using a desalting column equilibrated with fluoride-free buffer. At least in the case of RcMn(II)-SOD, the addition of 100 mM fluoride to a fresh sample did not result in Mn(II) release, rather it appeared that the repetitive melting−freezing cycles necessary to construct the titration curve using the same sample appeared to damage a small number of the RcMn(II)SOD centers leading to Mn-(II) release. The lower inset in Figure 6 shows the fluoride concentration dependence of the amplitude of the lowest-field RcMn(II)SOD hyperfine resonance. The changes rose to a maximum at about 100 mM fluoride concentration. The same variation in intensity was observed for the other low-field hyperfine resonances.

The simulations of the spectra of RcMn(II)SOD in the presence of saturating concentrations of fluoride were poor, and it was concluded that they could not be reliably fit with a single set of spin parameters. This suggested that fluoride was not capable of uniformly binding to all of the metal centers and that, similar to azide, only partial binding occurred even under saturating concentrations. As an initial guess, we assumed that each spectrum in Figure 6 was composed of only two components, the spectrum of the native RcMn(II)SOD and that of the putative fluoride−RcMn(II)SOD complex. A direct consequence of this assumption was that all of the spectra from the titration curve could be expressed as a linear combination of the native spectrum and the spectrum obtained with 100 mM fluoride. We verified that this was indeed the case using digital subtraction and that the initial assumption was correct. From the difference spectra we were able to deduce the spectrum of the fluoride−RcMn(II)SOD complex (see Figure S3, Supporting Information). The quantity of fluoride-coordinated Mn(II) centers under saturating conditions was determined to be about 50%. A titration curve based on this two-component analysis was essentially identical to the one obtained from peak intensities. Fit to a single-site binding model yielded a K_d of 9 mM.

Simulations of the spectrum of the putative fluoride−RcMn(II)SOD complex were of reasonable quality and yielded a $|D|$ value of 10.785 GHz and E of 0.626 GHz (Table 2 and Figure S3, Supporting Information). This meant that the $|D|$ value remained approximately unchanged compared to the native protein, while the E value increased by at least 0.10 GHz with fluoride binding (Table 2).

For the fluoride−EcMn(II)SOD complex, we took the same approach. Although the fluoride-free and 50 mM fluoride spectra were clearly different, there was a fortuitous overlap of the resonances that made it difficult to distinguish the components. To circumvent this problem, we serially subtracted different portions of the fluoride-free spectrum from the 50 mM fluoride spectrum and then attempted to simulate each of the difference spectra. To improve reliability, we simultaneously fitted the 285 and 190 GHz data. Only the difference spectra corresponding to 40−60% binding could be adequately simulated. The best fit was obtained for the spectrum corresponding to 50% binding. The only significant discrepancy was the presence of a six-line component corresponding to NPB Mn(II) ions (see Figure S4, Supporting Information). For EcMn(II)SOD, fluoride binding induced an increase in $|D|$ of 0.30 GHz and a decrease in E of 0.40 GHz resulting in $|D|$ and E values of 10.982 and 0.457 GHz, respectively (Table 2). These offsetting changes were the reason the resonances arising from fluoride-free and fluoride-complexed Mn(II) centers were so strongly overlapped.

Distinct from RcMnSOD and EcMnSOD, the addition of 20 mM fluoride to EcMn(Fe)SOD produced a spectrum that could be readily simulated (Figure 4). This was a good indication that the spectrum was dominated by a single component. The apparent K_d appeared to be below 5 mM. However, above 20 mM, the spectra underwent further small changes. Further titration studies will need to carried out to better characterize the effect of fluoride on the EcMn(Fe)-SOD protein. Simulations showed that after fluoride addition $|D|$ decreased by 0.25 GHz and E increased by 0.20 GHz (Table 2).

Specific and Nonspecific Anion Effects. To determine whether the effects of azide and fluoride were specific, the spectra of EcMnSOD with 100 mM sodium chloride or sodium sulfate were taken. Figure 7 shows the first four lines of the HFEPR spectra of the EcMn(II)SOD in the presence of different anions. At high azide concentrations (Figure 7), the first peak moved toward lower field and the second remained essentially unchanged. Essentially, the same effect was induced by the addition of 100 mM sodium chloride, but unlike azide, no evidence of six-coordinate Mn(II) was observed. Simulations showed that this change corresponded to an increase of E of about 0.10 GHz and no change in $|D|$ (Figure 7 and Table 2). Although the peak positions remained unchanged with fluoride addition, substantial changes inline occurred (see above). Sodium sulfate did not induce changes in the spectra (Figure 7). Hence, it was concluded that fluoride, chloride, and azide indeed exerted a specific effect on the pentacoordinate metal site but not sulfate, indicating that size might be an important factor.

DISCUSSION

Of the three effects studied, azide-induced changes in the HFEPR spectra were the easiest to understand. The appearance of a narrow six-line spectrum, the amplitude of which depended on azide concentration, was indicative of a large reduction in the zero-field interaction associated with the formation of hexacoordinated Mn(II) centers (*40*, *42*). Such centers have already been seen in the crystallographic structures of the *T. thermophilus* MnSOD protein in which the azide is the sixth ligand and is hydrogen-bonded to Tyr34

(*30*). Such centers were earlier proposed for FeSOD (*34*). What was surprising was that aside from EcMnSOD and RcMnSOD, none of the other three proteins formed hexacoordinate centers, even PgMnSOD proteins that were inhibited by azide (Table 1). In these latter cases, it must be assumed that azide binds only to Mn(III) or its point of interaction with the protein is sufficiently far from the metal binding center so as not to modify its electronic structure, and yet still be inhibiting (see below). Hence, the correlation between the capacity of a Mn(II)-containing SOD to form an azide−metal complex and to bind superoxide, although attractive, cannot be so simple.

What was equally surprising was that HFEPR spectra showed that although EcMnSOD, RcMnSOD, and both PgMnSOD proteins were inhibited by fluoride (Table 1) none of the five proteins formed hexacoordinate centers in the presence of fluoride. Hexacoordinated centers involving this anion have been proposed for FeSOD (*35*). However, it is clear from the HFEPR spectra that in all five cases the fluoride anion does affect the zero-field interaction of the Mn(II) centers in a well-defined manner, but to an extent that was much smaller than in the case of hexacoordinate azide complex formation. Control experiments with sulfate and chloride and different buffer conditions showed that these effects were specific to the fluoride anion. Each of the spectra obtained during the course of the fluoride titration measurements could be decomposed into the native protein spectrum and a second spectrum of a different Mn(II) center that had a smaller $|D|$ and larger E (Table 2, Figures 6, and Figures S3 and S4, Supporting Information).

What is the relationship between the fluoride-induced spectroscopic changes and the electronic structure? For all five proteins, their $|D|$ values indicated that the Mn(II) centers remained pentacoordinate in the presence of fluoride (*42*). Moreover, since the fluoride-induced spectral changes were so well-defined, it can be assumed that they originated from a fluoride ion that had a fixed location in the protein. To gain a more quantitative picture of this effect, we turned to the relatively simple point-charge model (PCM) developed by Roelfsema and den Hartog (*50*). According to this model, the zero-field contribution of a point-charge at a distance R from the Mn(II) center is given by

$$D = 9.76\ \text{GHz}\ \text{Å}^3\left(\frac{3\cos^2\theta - 1}{R^3}\right)$$

and

$$E = 9.76\ \text{GHz}\ \text{Å}^3\left(\frac{\sin^2\theta\cos 2\phi}{R^3}\right) \qquad (2)$$

where R is the distance in Å and θ and φ are the polar angles relative to the zero-field axis system. The parameters leading to the numerical prefactor were estimated assuming a particular symmetry of the Mn(II) ligand field (*51*). However, it is thought that the value of the prefactor is not particularly sensitive to this assumption (*51*). The model does not adequately account for the primary ligand shell of SODs. This may be due to its purely point-charge (ionic) nature which would account for its success in rationalizing the Mn(II) D and E of ionic crystals (*50*, *52*, *53*). The R^{-3} dependence is close to the $R^{-2.5}$ that we previously estimated based on the temperature dependence of the MnSOD D zero-field parameter (*42*).

It is particularly illustrative to consider the first application of the PCM. In Mn(II)-doped $SrCl_2$ crystals, the D was found to be essentially zero, but an applied electric-field of 2.4×10^7 V/m caused D to increase by 0.030 GHz. Using the PCM and summing over 10^5 ions, Roeslfsema and den Hartog found that such an increase in D could be explained by a shift of Mn(II) by 0.11−16 Å induced by the electric field (*50*). One can draw some interesting parallels between this ionic crystal example and the situation with fluoride in MnSODs. In the latter, a nearby fluoride ion could play both roles, an indirect one as the source of the electric-field that can electrostatically affect the positions of the ligands relative to the Mn(II) center and a direct one as a newly introduced "lattice" ion. It is known that small displacements of ligands on the order of few hundreds of angstroms can cause changes in D of more than 0.20 GHz (*42*).

Although the indirect effect of a fluoride anion on the structure of the primary ligand sphere is difficult to quantitate, the R^{-3} dependence of the direct charge effect does put reasonable restrictions on where the fluoride anion could be bound. If one assumes eq 2 is directly applicable, ionic effects beyond 6 Å will not have been detectable by our experiments. If in the unlikely event that the numerical prefactor were an order of magnitude larger, then the distance limited would have been double. Within a 6 Å range, there are several sites that a fluoride anion can bind through hydrogen-bonding/electrostatic interactions, but within the putative access channel, the most likely locations were His30 and Tyr34. As described above, the same Tyr34 hydrogen-bonds the azide ligand of the azide−MnSOD complex (*30*). The sizes of the zero-field parameters indicate that it is unlikely that a fluoride anion can occupy the same position as Mn(II)-ligating azide nitrogen. To obtain estimates of what the zero-field parameters might be for a hexacoordinated fluoride−Mn(II)SOD complex, we used the Superposition Model (*42*, *54*, *55*). We have previously shown that this model can adequately account for the zero-field parameters of the hexacoordinated azide−EcMn(II)SOD complex. The predicted zero-field parameters for the fluoride complex were 1.55 GHz for $|D|$ and 0.25 GHz for E, if one assumed that the ligand sphere geometry was the same as for the azide complex. This predicted D value is more than a factor of 6 smaller than observed. In contrast, if the fluoride anion were to occupy the same position as the middle azide nitrogen in the azide−EcMn(II)SOD complex, the effect would be purely electrostatic and would be relatively small. The PCM predicts that the D and E values for the fluoride complex would differ from native pentacoordinate values by only −0.22 and 0.25 GHz, respectively, assuming the zero-field axis coincides with Mn(II)-solvent direction. The opposite signs for the D and E values were due to their respective angular dependences. At the position of the furthest azide nitrogen atom from the metal ion, the fluoride contribution would drop to −0.08 and 0.10 GHz, for D and E, respectively. Thus, the predicted effect of a point charge on the zero-field parameters at a position comparable to that of the middle azide nitrogen was in reasonable agreement in magnitude with the experimental data. Hence, according to the point charge model, a fluoride anion hydrogen-bonded

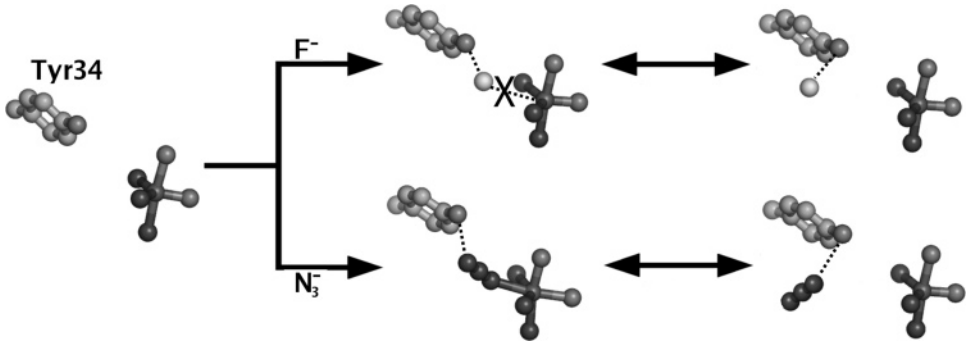

FIGURE 8: A model of fluoride and azide binding in MnSODs. In its inner-sphere position (middle), an azide molecule can directly bond the Mn(II) center and hydrogen-bond Tyr34. The fluoride anion is too small and only forms a hydrogen bond to Tyr34 but lies close to the metal ion. For both anions, the proposed second site is an outer-sphere one with the anion hydrogen-bonded to Tyr34 pointing away from the metal (right).

to Tyr34 pointing toward, but not directly bonded to the metal ion, seems quite reasonable (Figure 8, middle).

Similarly, the PCM could also be used to rationalize the smaller effects of azide and chloride anions. In these cases, the binding sites must have been further away, for example, on His30 or on Tyr34, but with the hydrogen-bounded anion pointing away from the Mn(II) site. Clearly, ongoing site-directed mutagenesis experiments on Tyr34 and other residues will provide more insights.

For Rc- and EcMnSOD, the effect of fluoride and azide on the HFEPR spectra became saturated well below 100% binding. For each anion, comparable amounts of binding were obtained for both Rc- and EcMnSOD. Incomplete anion binding due to nonspecific structural heterogeneity could not be rigorously ruled out. It is worth noting that, even in the crystallographic structure of *T. thermophilus* azide−MnSOD complex, azide occupied only 51% of the centers (*30*), while in the fluoride−FeSOD structure of *E. coli*, the occupancy was 70% (*35*). If such structural heterogeneities were present, it was neither damaging nor irreversible at the level of activity and the structural integrity of the metal binding site, since samples used for these experiments could be washed and reused without significant loss of activity or spectral intensity. An alternative and more likely explanation was structural heterogeneity in the form of multiple protein states or multiple anion binding sites. This was evident in the azide−EcMn(II)SOD titration experiments where anion addition led to the reversible formation of both hexacoordinated Mn(II) centers and pentacoordinated sites with modified zero-field interaction. The latter may be indicative of structural modifications induced by high anion concentrations that may limit direct binding to the metal or, alternatively, of a second distal binding site. In either case, the site of binding or modification must have been distant from the Mn(II) since its effect on the Mn(II) HFEPR spectrum was so small. A rough approximation based on the PCM puts the distance at greater than 6 Å. We have already established that at temperatures near freezing both EcMn(II)SOD and RcMn(II)SOD do indeed exist in two states, a hexacoordinate/pentacoordinate Mn(II) equilibrium (see Supporting Information and ref *42*). We have speculated that the equilibrium involves the motion of one of the structural water molecules from its position in the access channel to the primary ligand shell of the metal binding site becoming the sixth ligand. The most likely candidates were either the water hydrogen-bonded to His30 or to Tyr34. The hydrogen-bonding sites in both cases were about 7 Å from the manganese center. Another example of a pentacoordinate to hexacoordinate transition was observed for the azide−EcMn(III)SOD complex at low temperatures (*38*, *39*). Hence, there appears to be good experimental evidence for two protein states or binding sites. A very simple two-site binding model is one in which the anion is hydrogen-bonded to Tyr34 but can occupy either an inner-sphere position or an outer-sphere one. In the former, the O_{Tyr35}−H···A$^-$ hydrogen bond points toward the Mn(II) ion (Figure 8, middle), while in the latter, the triad of atoms points away from the metal center with the anion furthest away (Figure 8, right).

If such a model is correct, then the superoxide ion should interact with the Tyr34 in much the same way. It is likely that the superoxide anion is also too short to directly bind to metal but would be sufficiently close for rapid electron transfer and direct proton transfer from Tyr34, which in turn could be reprotonated by a nearby water molecule. The resulting peroxide could then be efficiently released from the active site, since it is not bonded to the metal. A variant of this model is one in which the superoxide molecule is hydrogen-bonded to both Tyr34 and the axial solvent ligand but does not bond to the metal ion. MnSOD crystal structures indicate that such a configuration is possible. If the axial solvent ligand were a water molecule, then this arrangement would facilitate both the rapid transfer of two protons, one from Tyr34 and another from the water ligand, and an electron while maintaining charge balance at the active site and facilitate the removal of the product. Such a role for Tyr34 in positioning the substrate and product has been previously suggested by others (*27*, *37*).

Since it is clear that anions can significantly modify the Mn(II)SOD zero-field splitting interaction, the effect of pH on the EcMn(II)(Fe)SOD spectrum can be understood in the same way, that is, the effect of a nearby pH-dependent appearance of a negative charge. All Mn/FeSODs have characteristic p*K* values. Depending on the metal and oxidation states, these p*K* values have been variously assigned to hydroxide binding (*19*, *20*, *23*), possible deprotonation of the solvent ligand (*39*), and deprotonation of Tyr34 (*21*−*23*, *25*, *28*, *29*). Interestingly, the only other spectrum affected by pH was that of PgMnSOD-G155T, which coincidentally was the only other protein with Fe-only activity. For the other three proteins, the spectra were independent of pH, except for the presence of a sharp six-line component that was indicative of the tendency of all of

the proteins to release Mn(II) at high pH. This was not unexpected since it is known that metal exchange can be achieved at high pH (*56*). In all five cases, the zero-field parameters indicated that the Mn(II) centers remain pentacoordinate even above pH 10. This conclusively ruled out ligation of an additional hydroxide to the Mn(II) center. The deprotonation of a water ligand seemed equally unlikely, since the appearance of an additional negative charge in the primary ligand shell should have modified the zero-field interaction both directly and indirectly by changing positions of the ligands. Simultaneous simulations of the 190 and 285 GHz EcMn(II)(Fe)SOD spectra showed that changes in $|D|$ and E were very similar in size to the effect of fluoride. The biggest difference was that both parameters required larger distributions to fit the high pH data (Figure 4 and Table 2). Hence, it was tempting to conclude that a residue became ionized at a distance comparable to the fluoride binding site.

The measured p*K* of 9.7 strongly suggests that a tyrosine was responsible for the observed pH effect. The only tyrosines within 7 Å of the Mn(II) are Tyr34 and Tyr76. The point charge contribution of the latter is predicted to be undetectably small due to its distance. For Tyr34, the contribution to D is predicted to be negligible because the Tyr34 phenoxyl oxygen atom lies very close to the "magic angle" with respect to the Mn(II)-solvent axis, where the angular term vanishes. However, it seems reasonable that the ionization of Tyr34 would also have a substantial indirect effect on the primary ligand shell, since it participates in the hydrogen-bond network that involved the axial water molecule.

The lack of a pH dependence in the case of EcMn(II)-SOD was in contradiction with the work by Maliekal and co-workers (*29*). Their Resonance Raman data indicated that the wild-type enzyme had two p*K* values, one at 10.0 and another at 10.7, while the EcMn(II)SOD-Tyr34Phe mutant had only a single p*K* at 10. Parallel 9 GHz EPR spectroscopy showed that EcMn(II)SOD-Tyr34Phe was unaffected by pH. For the wild-type, the intensity of the broad component corresponding to the native enzyme decreased with increasing pH with a concomitant increase in a six-line component centered at the magnetic-field corresponding to a *g*-value of 4 ($g = 4$) (*29*). A p*K* of 10.2 was obtained from the 9 GHz EPR data. Differences in pH dependence of the Resonance Raman and EPR spectra were attributed to the deprotonation of Tyr34 and concurrent changes induced by the tyrosine deprotonation on the Mn(II) ligand sphere either in the axial solvent position or the coordination of a new water molecule as a sixth-ligand. Such changes in the ligand sphere are inconsistent with our HFEPR spectra of EcMn(II)SOD at high pH, since the HFEPR spectra taken at pH 11 were exactly identical to those recorded at pH 8 with the exception of an increased presence of NPB Mn(II) (Figure 2). Moreover consistent with our HFEPR measurement, our 9 GHz spectra were not pH-dependent, and the $g = 4$ component was not detected.

The complexity of the 9 GHz Mn(II)SOD EPR spectra makes specific effects difficult to interpret and assign (see discussion in Supporting Information). This is the case for the high-pH $g = 4$ resonances. Only two types of Mn(II) centers were observed in our high pH 285 GHz EcMn(II)-SOD spectra, the pentacoordinated centers and NPB Mn-(II). The presence of NPB ions was unambiguously identified by HFEPR spectroscopy in the filtrate of the pH 11 EcMn-(II)SOD sample (Figure 2, top trace). The filtrate spectrum exactly matched the six-line component observed in the high pH EcMn(II)SOD spectrum. We found that under certain conditions NPB Mn(II) ions in the MnSOD samples can contribute a $g = 4$ six-line component to the 9 GHz spectra. In particular, in our experiments, EDTA was required (see Supporting Information). Hence, the HFEPR and 9 GHz measurements strongly suggest that the high-pH $g = 4$ resonances observed in the previous study were probably due to NPB Mn(II) rather than to protein-based Mn(II) specific to high-pH. The absence of such signals in high-pH samples of the Tyr34Phe mutant noted in the previous study (*29*) is not that remarkable. As can be seen from the various examples given in the Supporting Information, factors such as species, buffer composition, and freezing regimes, among others, greatly affected the levels of NPB Mn(II). It is also interesting to note that the same mutation in the human MnSOD is known to lead to a thermally more stable protein (*28*).

It is also not clear from the previous 9 GHz EcMn(II)-SOD titration data whether the pH-dependent amplitude changes were indeed titratable events, since no plateau appeared to be reached at high pH (*29*). The only discernible changes in the EcMn(II)MnSOD HFEPR spectra correlated with increasing pH were due to the continuous release of Mn(II). This again points to NPB Mn(II) as source of the pH-dependent changes observed in the previous work. It is also important to note that one method for removing the metal ion in Mn- and FeSODs involves high pH treatment (*56*). If the source of the high-pH resonances was indeed NPB Mn(II) and both the EPR and Resonance Raman samples that were used in the previous study contained such centers, then the discrepancy between Maliekal's results and ours could arise from the possibility that the p*K* at 10.7 detected by Resonance Raman corresponded only to the deprotonation of Tyr34 in non-manganese-containing proteins.

If the pH-dependent changes in the EcMn(II)(Fe)SOD spectra are indeed due to deprotonation of Tyr34, then the lack of such a dependence for EcMn(II)SOD implies that the Tyr34 in this protein remains protonated even above pH 11. The p*K* of EcFe(II)(Mn)SOD, the iron-reconstituted manganese protein, has been previously shown to be 9.2 (*57*). This p*K* difference is also mirrored in the case of EcFe(II)-SOD and its manganese-substituted form. The native EcFe-(II)SOD has a pK_a of 8.5 (*21*), which changes to 9.8 when reconstituted with Mn(II) (see above). Hence, the Tyr34 pK_a is apparently lower with Fe(II) than with Mn(II) in the active site (*29*). The metal ion is in effect electrostatically connected to the Tyr34 through the hydrogen-bonding network that connects the two via the axial solvent, ligand, and an intervening Gln146 residue. In wild-type PgSOD, the solvent−Gln146 and Gln146−Tyr34 distances are nearly equal, 2.93 and 2.99 Å (*43*), respectively, as is the case in EcMnSOD, except with distances of 2.90 and 2.99 Å (*58*), respectively. For the iron-only active proteins, the hydrogen-bonding balance favors Tyr34. In PgSOD-G155T, the distance from Gln146 to Tyr34 is 2.98 Å (*43*), while from Gln146 to the solvent molecule it is 3.11 Å. In EcFeSOD, the distances are 3.11 and 3.41 Å, respectively (*30*). Since the hydrogen-bonding favors Tyr34 in these latter two cases,

one might expect the Tyr34 in iron-only active proteins to have a lower pK_a.

In summary, it is interesting to note trends among the series of proteins regarding metal specific activity. EcMn-SOD and RcMnSOD had high activity with manganese, but low or no activity with Fe at neutral pH, and they were characterized by (1) HFEPR spectra unaffected by pH, (2) formation of hexacoordinated complexes below 0 °C without exogenous ligands, and (3) formation of hexacoordinate with addition of azide. By comparison, EcMn(Fe)SOD and PgMnSOD-G155T had little or no activity with manganese, were affected by pH, but did not bind azide. The fully cambialistic wild-type *P. gingivalis* enzyme appeared to be intermediate with a very small, but reproducible, effect of pH but unaffected by azide or fluoride. The differences between RcMnSOD and PgMnSOD suggest that cambialistic enzymatic activity is not a product of a unique type of active site structure but is conferred by a multiplicity of factors.

ACKNOWLEDGMENT

L.C.T. and N.C. acknowledge the support of CONICET, SeTCIP, and ANPCyT (PICT-8753 and PICT-5105) from Argentina and the ECOS Sud/SeCyT collaboration program (Project A02B01). The authors thank J. Colin for assistance in obtaining the 9 GHz spectra. S.U. is grateful to F. Leach and A.W. Rutherford for support and encouragement.

SUPPORTING INFORMATION AVAILABLE

Figures and discussion relating to the identification of protein- and nonprotein-bound manganese; comparison of 9 and 285 GHz spectra of MnSOD; identification of the spectrum of the putative Mn(II)SOD−fluoride complex; pH dependence of the 9 and 284 GHz EcMn(II)SOD EPR spectra and $g = 4$ resonances in the 9 GHz spectra of pH 10 EcMnSOD in the presence of free Mn(II) and EDTA. This material is available free of charge via the Internet at http://pubs.acs.org.

REFERENCES

1. Fridovich, I. (1995) Superoxide radical and superoxide dismutases, *Annu. Rev. Biochem. 64*, 97−112.
2. Touati, D. (1997) Superoxide dismutases in bacteria and pathogen protists, in *Oxidative Stress and the Molecular Biology of Antioxidant Defenses* (Scandalios, J. G., Ed.) pp 447−493, Cold Spring Harbor, New York.
3. Bull, C., and Fee, J. A. (1985) Steady-state kinetic studies of superoxide dismutases: Properties of the iron containing protein from *Escherichia coli*, *J. Am. Chem. Soc. 107*, 3295−3304.
4. Lavelle, F., McAdam, M. E., Fielden, E. M., and Roberts, P. B. (1977) A pulse-radiolysis study of the catalytic mechanism of the iron-containing superoxide dismutase from *Photobacterium leiognathi*, *Biochem. J. 161*, 3−11.
5. Klug-Roth, D., Fridovich, I., and Rabani, J. (1973) Pulse radiolytic investigations of superoxide catalyzed disproportionation. Mechanism for bovine superoxide dismutase, *J. Am. Chem. Soc. 95*, 2786−2790.
6. Kim, E. J., Chung, H. J., Suh, B., Hah, Y. C., and Roe, J. H. (1998) Transcriptional and post-transcriptional regulation by nickel of sodN gene encoding nickel-containing superoxide dismutase from *Streptomyces coelicolor* Muller, *Mol. Microbiol. 27*, 187−195.
7. Kim, F. J., Kim, H. P., Hah, Y. C., and Roe, J. H. (1996) Differential expression of superoxide dismutases containing Ni and Fe/Zn in *Streptomyces coelicolor*, *Eur. J. Biochem. 241*, 178−185.
8. Stroupe, M. E., DiDonato, M., and Tainer, J. A. (2001) in *Handbook of Metalloproteins* (Messerschmidt, A., Huber, R., Wieghardt, K., and Paulos, T., Eds.) pp 941−951, Wiley and Sons, Chichester, U.K.
9. Miller, A.-F. (2001) in *Handbook of Metalloproteins* (Messerschmidt, A., Huber, R., Wieghardt, K., and Paulos, T., Eds.) pp 668−682, Wiley and Sons, Chichester, U.K.
10. Sugio, S., Hiraoka, B. Y., and Yamakura, F. (2000) Crystal structure of cambialistic superoxide dismutase from *Porphyromonas gingivalis*, *Eur. J. Biochem. 267*, 3487−3495.
11. Schmidt, B., Meier, B., and Parak, F. (1996) X-ray structure of the cambialistic superoxide dismutase from *Propionibacterium shermanii* active with Fe or Mn, *J. Biol. Inorg. Chem. 1*, 532−541.
12. Ose, D. E., and Fridovich, I. (1976) Superoxide dismutase. Reversible removal of manganese and its substitution by cobalt, nickel or zinc, *J. Biol. Chem. 251*, 1217−1218.
13. Yamakura, F. (1980) Cadmium, chromium, and manganese replacement for iron in iron-superoxide dismutase from *Pseudomonas ovalis*, *J. Biochem. (Tokyo) 88*, 191−196.
14. Meier, B., Barra, D., Bossa, F., Calabrese, L., and Rotilio, G. (1982) Synthesis of either Fe- or Mn-superoxide dismutase with an apparently identical protein moiety by an anaerobic bacterium dependent on the metal supplied, *J. Biol. Chem. 257*, 13977−13980.
15. Amano, A., Shizukuishi, S., Tamagawa, H., Iwakura, K., Tsunasawa, S., and Tsunemitsu, A. (1990) Characterization of superoxide dismutase purified from either anaerobically maintained or aerated *Bacteroides gingivalis*, *J. Bacteriol. 172*, 1457−1463.
16. Martin, M. E., Byers, E. B. R., Olson, M. O. J., Salin, M. L., Arceneaux, J. E. L., and Tolbert, C. (1986) A *Streptococcus mutans* superoxide dismutase that is active with either manganese or iron as a cofactor, *J. Biol. Chem. 261*, 9361−9367.
17. Gregory, E. M. (1985) Characterization of the O_2-induced manganese-containing superoxide dismutase from *Bacteroides fragilis*, *Arch. Biochem. Biophys. 238*, 83−89.
18. Tabares, L. C., Bittel, C., Carrillo, N., Bortolotti, A., and Cortez, N. (2003) The single superoxide dismutase of *Rhodobacter capsulatus* is a cambialistic, manganese-containing enzyme, *J. Bacteriol. 185*, 3223−3227.
19. Fee, J. A., McClune, G. J., O'Neill, P., and Fielden, E. M. (1981) Saturation behavior of superoxide dismutation catalyzed by the iron containing superoxide dismutase of *E. coli* B, *Biochem. Biophys. Res. Commun. 100*, 377−384.
20. Tierney, D. L., Fee, J. A., Ludwig, M. L., and Penner-Hahn, J. E. (1995) X-ray absorption spectroscopy of the iron site in *Escherichia coli* Fe(III) superoxide dismutase, *Biochemistry 34*, 1661−1668.
21. Sorkin, D. L., Duong, D. K., and Miller, A. F. (1997) Mutation of tyrosine 34 to phenylalanine eliminates the active site p*K* of reduced iron-containing superoxide dismutase, *Biochemistry 36*, 8202−8208.
22. Sorkin, D. L., and Miller, A. F. (1997) Spectroscopic measurement of a long-predicted active site p*K* in iron-superoxide dismutase from *Escherichia coli*, *Biochemistry 36*, 4916−4924.
23. Jackson, T. A., Xie, J., Yikilmaz, E., Miller, A. F., and Brunold, T. C. (2002) Spectroscopic and computational studies on iron and manganese superoxide dismutases: Nature of the chemical events associated with active-site p*K*s, *J. Am. Chem. Soc. 124*, 10833−10845.
24. Terech, A., Pucheault, J., and Ferradini, C. (1983) Saturation behavior of the manganese-containing superoxide dismutase from *Paracoccus denitrificans*, *Biochem. Biophys. Res. Commun. 113*, 114−20.
25. Hsu, J. L., Hsieh, Y., Tu, C., O'Connor, D., Nick, H. S., and Silverman, D. N. (1996) Catalytic properties of human manganese superoxide dismutase, *J. Biol. Chem. 271*, 17687−17691.
26. Borgstahl, G. E. O., Pokross, M., Chehab, R., Sekher, A., and Snell, E. H. (2000) Cryo-trapping the six-coordinate, distorted-octahedral active site of manganese superoxide dismutase, *J. Mol. Biol. 296*, 951−959.
27. Whittaker, M. M., and Whittaker, J. W. (1997) Mutagenesis of a proton linkage pathway in *Escherichia coli* manganese superoxide dismutase, *Biochemistry 36*, 8923−8931.
28. Guan, Y., Hickey, M. J., Borgstahl, G. E. O., Hallewell, R. A., Lepock, J. R., O'Conner, D., Hsieh, Y., Nick, H. S., Silvermann, D. N., and Tainer, J. A. (1998) Crystal structure of Y34F mutant human mitochondrial manganese superoxide dismutase and the functional role of tyrosine 34, *Biochemistry 37*, 4722−4730.
29. Maliekal, J., Karapetan, A., Vance, C., Yikilmaz, E., Wu, Q., Jackson, T., Brounold, T. C., Spiro, T. G., and Miller, A.-F. (2002)

Comparison and contrasts between the active site PKs of Mn-superoxide dismutase and those of Fe-superoxide dismutase, *J. Am. Chem. Soc. 124*, 15064−15075.
30. Lah, M. S., Dixon, M. M., Pattridge, K. A., Stallings, W. C., Fee, J. A., and Ludwig, M. L. (1995) Structure−function in *Escherichia coli* iron superoxide dismutase: Comparisons with the manganese enzyme from *Thermus thermophilus*, *Biochemistry 34*, 1646−1660.
31. Ludwig, M. L., Metzger, A. L., Pattridge, K. A., and Stallings, W. C. (1991) Manganese superoxide dismutase from *Thermus thermophilus*. A structural model refined at 1.8 Å resolution. *J. Mol. Biol. 219*, 335−358.
32. Stallings, W. C., Metzger, A. L., Pattridge, K. A., Fee, J. A., and Ludwig, M. L. (1991) Structure−function relationships in iron and manganese superoxide dismutases, *Free Radical Res. Commun. 12−13* (Pt. 1), 259−268.
33. Whittaker, M. M., and Whittaker, J. W. (1991) Active site spectral studies on manganese superoxide dismutase, *J. Am. Chem. Soc. 113*, 5528−5540.
34. Slykhouse, T. O., and Fee, J. A. (1976) Physical and chemical studies on bacterial superoxide dismutases, *J. Biol. Chem. 251*, 5472−5477.
35. Schmidt, M. (1999) Manipulating the coordination mumber of the ferric iron within the cambialistic superoxide dismutase of *Propionibacterium shermanii* by changing the pH-value. A crystallographic analysis. *Eur. J. Biochem. 262*, 117−127.
36. Whittaker, J. W., and Solomon, E. I. (1988) Spectroscopic studies on ferrous non-heme iron active sites: Magnetic circular dichroism of mononuclear Fe sites in superoxide dismutase and lipoxygenase, *J. Am. Chem. Soc. 110*, 5329−5339.
37. Miller, A. F., Sorkin, D. L., and Padmakumar, K. (2005) Anion binding properties of reduced and oxidized iron-containing superoxide dismutase reveal no requirement for tyrosine 34, *Biochemistry 44*, 5969−5981.
38. Whittaker, M. M., and Whittaker, J. W. (1996) Low-temperature thermochromism marks a change in coordination for the metal ion in manganese superoxide dismutase, *Biochemistry 35*, 6762−6770.
39. Jackson, T. A., Karapetan, A., Miller, A.-F., and Brunold, T. C. (2004) Spectroscopic and computational studies of the azide-adduct of manganese superoxide dismutase: Definitive assignment of the ligand responsible for the low-temperature thermochroism, *J. Am. Chem. Soc. 126*, 12477−12491.
40. Un, S., Dorlet, P., Voyard, G., Tabares, L. C., and Cortez, N. (2001) High-field EPR characterization of manganese reconstituted superoxide dismutase from *Rhodobacter capsulatus*, *J. Am. Chem. Soc. 123*, 10123−10124.
41. Un, S., Tabares, L. C., Cortez, N., Hiraoka, B. Y., and Yamakura, F. (2004) Manganese(II) zero-field interaction in cambialistic and manganese superoxide dismutases and its relationship to the structure of the metal binding site, *J. Am. Chem. Soc. 126*, 2720−2726.
42. Tabares, L. C., Cortez, N., Agalidis, I., and Un, S. (2005) Temperature-dependent coordination in *E. coli* manganese superoxide, *J. Am. Chem. Soc. 127*, 6039−6047.
43. Yamakura, F., Sugio, S., Hiraoka, B. Y., Yokota, T., and Ohmori, D. (2003) Pronounced conversion of the metal-specific activity of superoxide dismutase from *Porphyromonas gingivalis* by the mutation of a single amino acid (Gly155Thr) located apart from the active site, *Biochemistry 42*, 10790−10799.
44. Cortez, N., Carrillo, N., Pasternak, C., Balzer, A., and Klug, G. (1998) Molecular cloning and expression analysis of the *Rhodobacter capsulatus* sodB gene, encoding an iron superoxide dismutase, *J. Bacteriol. 180*, 5413−5420.
45. McCord, J. M., and Fridovich, I. (1969) Superoxide dismutase. An enzymic function for erythrocuprein (hemocuprein), *J. Biol. Chem. 244*, 6049−6055.
46. Un, S., Dorlet, P., and Rutherford, A. W. (2001) A high-field tour of radicals in photosystems I and II, *Appl. Magn. Reson. 21*, 341−361.
47. Burghaus, O., Plato, M., Rohrer, M., Moebius, K., MacMillan, F., and Lubitz, W. (1993) 3-mm high-field EPR on semiquinone radical anions Q(.-) related to photosynthesis and on the primary donor P(.+) and acceptor QA(.-) in reaction centers of *Rhodobacter sphaeroides* R-26, *J. Phys. Chem. 97*, 7639−7647.
48. Markham, G. D., Rao, B. D. N., and Reed, G. H. (1979) Analysis of EPR powder patter lineshapes for Mn(II) including third-order perturbation corrections. Applications to Mn(II) complex with enzymes, *J. Magn. Reson. 33*, 592−602.
49. Beyer, W. F., Jr., and Fridovich, I. (1987) Effect of hydrogen peroxide on the iron-containing superoxide dismutase of *Escherichia coli*, *Biochemistry 26*, 1251−1257.
50. Roelfsema, K. E., and den Hartog, H. W. (1976) Splitting of the 6S5/2 state of substitutional Mn^{2+} in $SrCl_2$ by applied field. *Phys. Rev. B: Solid State 13*, 2723−2728.
51. Hagston, W. E., and Lowther, J. E. (1973) Relativistic effect in the ground-state splitting parameters of Mn^{2+} ions, *J. Phys. Chem. Solids 34*, 1773−1777.
52. Tanaka, K., Oomori, Y., Inoue, H., Kawano, K., Nakata, R., and Sumita, M. (1993) ESR studies of Mn^{2+} centres in $Sr_{1-x}Ba_xF_2$: Mn crystals, *J. Phys. Chem. Solids 54*, 315−323.
53. Tanaka, K., Suzuki, H., Kawano, K., and Nakata, R. (1995) ESR studies of Mn^{2+}-Ba centres in $Ca_{1-x}Ba_xF_2$:Mn, *J. Phys. Chem. Solids 56*, 703−714.
54. Heming, M., Remme, S., and Lehmann, G. (1986) Correlation of zero-field splittings and site distortions. X. Complexes of Mn^{2+} with mixed ligands, *J. Magn. Reson. 69*, 134−143.
55. Newman, D. J., and Urban, W. (1975) Interpretation of *S*-state ion EPR spectra, *Adv. Phys. 24*, 793−844.
56. Yamakura, F. (1978) A study on the reconstitution of iron-superoxide dismutase from *Pseudomonas ovalis*, *J. Biochem. 83*, 849−857.
57. Vance, C. K., and Miller, A. F. (1998) Spectroscopic comparisons of the pH dependencies of Fe-substituted (Mn)superoxide dismutase and Fe-superoxide dismutase, *Biochemistry 37*, 5518−5527.
58. Edwards, R. A., Baker, H. M., Whittaker, M. M., Whittaker, J. W., Jameson, G. B., and Baker, E. N. (1998) Crystal structure of *Escherichia coli* manganese superoxide dismutase at 2.1 Å resolution, *J. Biol. Chem. 3*, 161−171.

BI051947M